Journal of Hydrology 572: 461-469 (2019)

Simultaneous estimation of the soil hydraulic conductivity and the van Genuchten water retention parameters from an upward infiltration experiment

Latorre, B., Moret-Fernández, D. *

Estación Experimental de Aula Dei, Consejo Superior de Investigaciones Científicas (CSIC), P.O. Box 202, 50059 Zaragoza, Spain;

* Corresponding author. E-mail: david@eead.csic.es Tel.: (+34) 976 71 61 40

ABSTRACT

This paper presents a new laboratory method to simultaneously estimate K_s and α and n parameters of the van Genuchten (1980) $\theta(h)$ from the inverse analysis of an upward infiltration curve measured in a 5-cm high soil column. The method was evaluated on synthetic 1D infiltration curves generated for a theoretical loamy sand, loam and clay soil. The influence of the soil initial condition on the inverse analysis was also studied. Next, an optimization method was presented and tested on eight theoretical soils (from loamy sand to clay). The method was subsequently applied to experimental curves measured on five sieved soils (from sand to clay) packed in 5-cm high and diameter cylinders. The K_s, α and n values estimated from the inverse analysis of the experimental curves were compared to those measured by Darcy and the pressure cell method (PC). The initial soil tension, h_i, which had an important influence on the optimization, was fixed to -6.0 10^5 cm. The optimization method resulted robust and allowed accurate estimates of the actual hydraulic parameters. A close to one relationship (R^2 = 0.99) was observed between the theoretical K_s, α and n and the corresponding values obtained with the inverse analysis. Regarding to the experimental soils, significant relationships close to one were obtained between K_s and n (R^2 > 0.98) estimated from inverse analysis and those measured with Darcy and PC. A non-significant relationship with slope away from one was found for α.

Keywords: Soil Hydraulic Properties; Sorptivity; Inverse Analysis; Richard’s Model.

1. INTRODUCTION

Characterization of the hydraulic conductivity, *K*, and the water retention curve, $\theta(h)$, is crucial to determine the water flow in the vadose zone. *K* is a measure of the soil ability to transmit water when soil is submitted to a hydraulic head gradient. This parameter depends on the soil water content, the pressure head and the flux across the boundary of a soil compartment (Dane and Hopmans 2002). The soil water retention curve describes the relationship between the volumetric water content, θ [L^3 L^{-3}], and the matric potential, *h* [L]. $\theta(h)$ depends upon the particle-size distribution, which determines the soil texture, and the arrangement of the solid particles, which refers to the soil structure (Dane and Hopmans, 2002). One of the most common functions used to describe $\theta(h)$ is the unimodal van Genuchten (1980) model, which is defined by the saturated (θ_s) and residual (θ_r,) volumetric water content and the empirical α and *n* factors. An additional *m* parameter, commonly defined as $m = 1 - \left(\frac{1}{n}\right)$, is also employed. θ_r is defined as the water content for which the gradient $d\theta/dh$ becomes zero (excluding the region near θ_s which also has a zero gradient), *n* [-] is the slope of $\theta(h)$ and is related to pore-size distribution, and α [L^{-1}] is a scale factor that defines the shape of $\theta(h)$ near θ_s.

The saturated hydraulic conductivity, K_s, can be measured with either the constant head or the falling-head method (Klute and Dirksen, 1986). The reference laboratory method used to determine $\theta(h)$ is the pressure extractor (Klute, 1986). Although this technique has been improved by incorporating alternative methods to determine θ (Jones et al., 2005; Moret-Fernández et al., 2012), the long time needed to conclude a measurement together with its limitations on fine textured soils (Solone et al., 2012) can restrict its use.

Other family of methods to estimate K and $\theta(h)$ are based on the inverse numerical analysis of Richard's transient water flows. The main advantage of these techniques is the simultaneous estimation of $\theta(h)$ and $K(h)$. To date, four different methods based on the inverse analysis of a transient water flow are available: evaporation and horizontal-, downward- and upward-infiltration processes. The evaporation method is based on the Wind (1968) formulation, where soil tension is measured within a vertical soil column as water evaporates from its surface using tensiometers installed at multiple depths, and water content and flux are determined by weighing the column. In more recent studies, Wind's method has been modified and simplified (e.g., Schindler, 1980; Simunek et al., 1996; Schindler and Müller, 2006; Schindler et al., 2010; Masaoka and Kosugi, 2018). The horizontal infiltration method is based on the Shao and Horton (1998) procedure, where the saturated hydraulic conductivity is measured by Darcy, and α and n van Genuchten (1980) parameters are estimated with an integral method that solves the problem of water absorption into a horizontal soil column. To this end, a soil column inserted in a 20 cm-length transparent cylinder should be used. The downward infiltration method analyzes cumulative infiltration rates measured with a disc infiltrometer at several consecutive tensions (Simunek and van Genuchten, 1997). The combination of multiple tension cumulative infiltration data with measured initial and final water contents yields unique solutions of the inverse problem for the unknown parameters. This method has been successfully used in several studies, such as Ramos et al. (2006), Caldwell et al. (2013) or Rashid et al. (2015), among others.

Up to date, different laboratory upward infiltration methods have been developed. Hudson et al. (1996) estimated $\theta(h)$ and $K(h)$ from the inverse analysis of an upward flow using a constant flux of water at the bottom of the soil sample. Young et al. (2002) combined the water cumulative flux and the soil pressure head measured by two tensiometers installed along a 15-cm-long soil column. Although this technique gave satisfactory results, the long soil columns used in the experiment together the use of tensiometers may prevent its use in undisturbed soil samples. Moret-Fernández et al. (2016b) developed a method where K_s was calculated according to the Darcy's law and the $\theta(h)$ parameters were estimated from the inverse analysis of a multiple tension water absorption curve. Although the method proved effective, the high negative pressure head needed at the beginning of the experiment restricted its use to sieved soils. Peña-Sancho et al. (2017) estimated the soil hydraulic properties from a capillary wetting process at saturation followed by an overpressure step and an evaporation process. In this case, K_s was calculated by Darcy and the hysteresis phenomenon was introduced using an empirical model. Finally, Moret-Fernández and Latorre (2017) estimated the $\theta(h)$ parameters from K_s measured by Darcy and the sorptivity, S, and β parameter (Haverkamp et al., 1994). In this case S and β were estimated from the inverse analysis of an upward infiltration curve. Although this technique was satisfactorily validated on 5-cm high theoretical and experimental soils, the employed formulation restricted its use to soils ranged from sand to silt textural classes (Lassabatere et al., 2009).

Although all above cited references show that the upward infiltration is an effective process to estimate $\theta(h)$ and $K(h)$, further efforts are needed to develop an alternative method that allows simultaneous estimate of all hydraulic properties, in any kind of soil and using short soil columns. This work presents a new method to determine K_s, α and n from the inverse analysis of an upward infiltration curve measured on a 5-cm high soil column. The method was firstly evaluated with a global analysis applied on upward infiltration curves generated by HYDRUS-1D for a loamy sand, loam and clay soil. The influence of the initial soil pressure head on the inverse analysis was also studied. Next, an optimization method was proposed and tested on eight theoretical soils. The method was finally applied on experimental infiltration curves measured on different sieved soils of known hydraulic properties.

2. MATERIAL AND METHODS

2.1. Theory

The one-dimensional water flow equation in a variably saturated rigid porous medium is defined by the Richards model

$$\frac{\partial \theta}{\partial t} = \frac{\partial}{\partial z}\left(K \frac{\partial h}{\partial z} + K \right) \tag{1}$$

where θ is the volumetric soil water content [L^3 L^{-3}], t is time [T], z is a vertical coordinate [L], positive upward, h is the soil-water pressure head [L] and K is the hydraulic conductivity [L T^{-1}].

The soil hydraulic functions can be described by the van Genuchten-Mualem functions (van Genuchten, 1980)

$$S_e(h) = \frac{\theta(h) - \theta_r}{\theta_s - \theta_r} = \left[1 + (\alpha h)^n\right]^{-m} \tag{2}$$

$$K(S_e) = K_s S_e^l \left[1 - \left(1 - S_e^{1/m}\right)^m\right]^2 \tag{3}$$

where S_e is the effective saturation [−], θ_s and θ_r are the saturated and residual water content, respectively, α [L−*1*] and n [−] are shape parameters, m=1−1/n, l is a pore-connectivity parameter and K_s is the saturated hydraulic conductivity. Similar to defined by Simunek et al. (1996, 1998), Simunek and van Genuchten et al. (1997) and Young et al. (2002), among others, l was fixed to 0.5. Because θ_r and θ_s can be easily measured at the beginning and the end of the experiment, respectively, the hydraulic characteristics defined by Eq. (2) and (3) were reduced to three unknown parameters: α, n and K_s. In our case, these equations represent the wetting branch of the unsaturated hydraulic properties.

The soil sorptivity, S, [L T$^{-0.5}$] is defined as the capacity of a porous medium to absorb liquid by capillarity (Philip, 1957). S, expressed as function of the van Genuchten (1980) parameters, results (Moret-Fernández, et al., 2017a)

$$S^2 = \frac{(1-m)K_s}{\alpha m(\theta_s - \theta_r)} \int_{\theta_i}^{\theta_s} [\theta_s + \theta - 2\theta_i] S_e^{1/2 - 1/m} \left[\left(1 - S_e^{1/m}\right)^{-m} + \left(1 - S_e^{1/m}\right)^{m} - 2 \right] d\theta \qquad (4)$$

where θ_i is the initial water content. The soil sorptivity expressed as function of an upward infiltration curve, S^*, can be expressed as (Moret-Fernández, et al., 2017a)

$$I = S^* \sqrt{t} - Ct \qquad (5)$$

where I [L] is the cumulative upward infiltration and C is a constant that is related to the soil hydraulic conductivity (Minasny and McBratney, 2000). This equation is only valid for short-medium infiltration times.

2.2. Numerical simulations

The synthetic upward infiltration data was generated using the HYDRUS-1D software (Simunek et al., 1996). The method was tested on eight theoretical soils (Carsel and Parrish, 1988) ranged from loamy sand to clay soil textural classes (Table 1).

A 5 cm-high soil column was discretized with a 1-D mesh of 1000 cells. Previous conducted numerical analysis demonstrated that, under this discretization, the solution was grid independent. The initial time step in the simulation, which value depended on the total infiltration time, varied from 10^{-5} s to 0.025 s for sand to clay, respectively. The tension at the base of the soil column was 0 cm. The evaporation rate was considered null and atmospheric conditions with a maximal tension of 0 cm was imposed at the top boundary. Time cero corresponded to the beginning of the upward infiltration process, and the simulation finished when the wetting front arrived to the soil surface.

2.3. Inverse analysis

The α, n and K_s parameters were calculated by minimizing an objective function, $\Phi(\alpha, n, K_s)$, that represents the difference between HYDRUS-1D simulated curves and synthetic or experimental infiltration data

$$\Phi = \sqrt{\frac{\sum_1^N \left(I_e(t_i) - I_s(t_i)\right)^2}{N}} \quad (6)$$

where N is the number of measured I values, $I_e(t_i)$ and $I_s(t_i)$ are specific measurements at time t_i. The values of the objective function were initially summarized as contours lines in the K_s-n, α-n, and K_s-α error maps, given in each plane the remaining theoretical hydraulic parameter. K_s, α and n values ranged from 10^{-5} to 10^{-2} cm s^{-1}, 0.01 to 0.1 cm^{-1}, and 1.01 to 3.0, respectively, and K_s and α were logarithmically sampled. The parameter combination for each response surface were calculated on a rectangular grid. Each parameter was discretized into 100 points, resulting in 10000 grid points for each response surface. These error maps were generated for a theoretical loamy sand, loam and clay soil.

The influence of the initial pressure head (h_i) on the global optimization was studied on a synthetic loam soil. Two different initial soil tensions were compared: -1.0 10^3, -6.0 10^5 cm. These h_i correspond to a soil sample in equilibrium with an atmosphere at 20 ºC and relatively humidity of ≈100 and 60%, respectively (RILEM, 1980).

Experimental data is subject to several sources of uncertainty (i.e. water level drop in the water reservoir, initial and final water content, etc.). Only the experimental error corresponding to the water level measurement in the water reservoir was considered. A preliminary experiment performed with a ±72 cm pressure transducer installed in a 1.9 cm-diameter water reservoir and connected to a 5 cm-diameter soil cylinder resulted in a soil water infiltration measurement uncertainty of ±0.02 mm. The change of the objective function (Eq. 5) associated to the uncertainty source was first calculated and superimposed on the response surfaces in the form of a contour line (0.02 mm).

The soil sorptivity defined in the cumulative upward infiltration curve (Eq. 5), S^*, was calculated by applying an objective function that calculates the squared difference between numerically generated and predicted cumulative infiltration curves, where we set it to be minimized based the target parameters (S,C).

2.4. Optimization method

Previous studies on upward infiltration processes (Moret-Fernández et al., 2016, Peña-Sancho et al., 2017) have shown ill-conditioned error maps with long ellipsoid contours or elongated valleys. Given that a brute-force search is time-consuming (Horst and Romeijn, 2002), local optimization methods should be employed. First-order optimization methods, like gradient descent, oscillate quickly across the valley but move slowly along the valley floor. This results in extremely low convergence. Newton methods overcome this problem relying on the two first derivatives of the function: the gradient and the Hessian (Avriel, 2003). In the case of the Richards equation, the gradient function is not given and it is computed numerically. Any noise in this calculation, such as that introduced by numerical simulation, amplifies when the Hessian is inverted and introduces noise and instabilities.

Random search (RS) is a family of stochastic optimization methods that do not require the gradient of the function to be optimized (Brooks, 1958). The basic RS algorithm can be described as follows:

1. Initialize x with a random position in parameter-space.
2. Until a termination criterion is met, repeat the following:
    1. Sample a new position y, moving x in a random direction a given fixed step
    2. If f(y) < f(x) then move to the new position by setting x = y

Adaptive Step Size Random Search (ASSRS) (Schumer and Steiglitz, 1968) attempts to heuristically adapt the step size to improve the performance of the search. Though ASSRS is quite effective in reducing the objective function during the initial search phases, the average linear convergence rate is rather slow for more precise solutions. In order to obtain accurate estimations, deterministic optimization techniques are needed (Haiping, 1996).

In this work, ASSRS was combined with a gradient search method. In each iteration, a random direction is first proposed and explored. Subsequently a deterministic direction is computed based on the linear regression of the last five successfully points and is also explored. In both cases, an initial step size of 10^{-3} is considered which is incremented exponentially while the error is reduced. The explored variables were transformed to the (0,1) interval using the following extreme values: K = [10^{-6}, 10^{-2}] cm s^{-1}, α = [10^{-3}, 0.5] cm^{-1}, n = [1.0, 3.5] and considering logarithmic transformations in the case of K and α. This transformation simplifies calculations, guarantees the same properties in all explored directions and allows to accurately explore physical variables covering several orders of magnitude.

2.5. Experimental validation

The experimental upward infiltration curves were measured with a sorptivimeter device (Moret-Fernández et al., 2017a). This consists of a saturated perforated base 5 cm-internal diameter (i.d.) that accommodates a stainless steel cylinder (5 cm-i.d. x 5 cm-high) that contains the soil sample. The bottom of the perforated base is connected to a Mariotte water supply reservoir (30 cm high, 1.9 cm-i.d). A ±7.2 kPa differential pressure transducer (Microswitch; Honeywell International Inc.) connected to a datalogger (CR1000; Campbell Scientist, Inc., Logan, UT, USA) was installed at the bottom of the water supply reservoir. The time interval of the water level measurements was 1 s. To minimize the water losses by evaporation, the surface of the soil column was covered with a lid. More details of the sorptivimeter can be found in Moret-Fernández et al. (2017a).

The upward infiltration method was applied on five 2-mm sieved soils with textural classes ranging from sand to clay (Table 2). The sieved material was initially stored at ≈ 20 ºC and ≈ 30% of relative humidity during several months. Since the soil is in equilibrium with the air in the chamber, the soil tension corresponding to this atmospheric condition is -1.6 10^6 cm (RILEM, 1980). The soils were next homogenously packet in 5-cm high and diameter cylinders and weighted. To this end, the sieved soil was poured in by hand and gently tapped in small incremental steps to achieve a uniform bulk density. This initial weight defined the residual gravimetric water content. Next, the cylinders were stored during several months at a temperature of ≈ 20 ºC and relative humidity of ≈ 60 %, which corresponds to a soil pressure head of -6.0 10^5 cm (RILEM, 1980). The upward infiltration started when the cylinder containing the soil was placed on the sorptivimenter, and finished when the wetting front arrived at the soil surface. At this time, the soil sample was saturated by raising the air inlet tube of the Mariotte reservoir to the soil surface. Once the soil sample was saturated, the core was disassembled, weighted, dried at 105 ºC during 24 h, and weighted again. Soils with high gypsum content (Table 1) were dried at 50 ºC during 48 h (Moret-Fernández et al. 2016b). The soil bulk density (ρ_b) was calculated as the product between the core volume and the dry-weight of the soil. θ_s and θ_r were calculated as the product between ρ_b and the corresponding gravimetric data. Once θ_s and θ_r calculated, K_s and α and n were finally estimated by applying the optimization method to the corresponding upward infiltration curves.

The K_s and α and n parameters estimated from the inverse analysis were compared with those calculated by Darcy and the pressure cell, PC, method (Moret-Fernández et al. 2012), respectively. The volumetric water content in the PC was measured by TDR at air-dried soil conditions, which corresponds to a pressure head (*h*) of approximately –1.6 MPa, at soil water saturation and at pressure heads of –0.5, –1.5, –3, –10 and –50 kPa. In this case, θ_r and θ_{sat} corresponded to the air-dried and saturated water content measured by TDR, respectively. The measured pairs of θ and h values were numerically fitted to the van Genuchten (1980) model (Eq. 2). To this end, θ_{sat} and θ_r were considered as known values, and α and n were estimated by minimizing an objective function that represents the difference between model and experimental data (Moret-Fernández et al., 2017b). The saturated hydraulic conductivity was estimated by the Darcy's law. Because the inverse analysis of upward infiltration curves and PC methods define the opposite branches of the water retention curve, α values obtained with PC were converted to the wetting branch of the water retention curve using the Gebrenegus and Ghezzehei (2011) hysteresis index.

3. RESULTS AND DISCUSSION

3.1. Synthetic soil analysis

The analysis of the results obtained on the synthetic loam soil shows that h_i had an important influence on the error maps (Fig. 1). When the initial tension is located in the transition zone of the water retention curve (i.e. -1.0 10^3 cm) (Fig. 1), small variations of n and α produce large changes in the initial soil water content. This translates into error maps with a focused minimum. Although the contour lines of the error maps tend to length when initial tension is shifted to the flat zone of the water retention curve (i.e. 6.0 10^{-5}), the minimum is still preserved (Fig. 1). These results indicate that very extremely negative h_i should not be employed. Overall, initial soil tension of -10^3 cm could be experimentally obtained with a pressure extractor. However, we discard this technique because the pressure plates method is not consistent in fine soils (Solone et al., 2012), and it has little effectiveness in long cores (i.e. 5 cm high), where the very long draining time needed to stabilize the water content into the soil core can restrict its use. On the other hand, the soil water draining process within the pressure plates, which can alter the soil structure by collapsing the more unstable soil macrostructure (Moret-Fernández et al. 2016a), can modify the actual soil hydraulic properties. In any case, the use of a pressure extractor would be only recommendable in very stable and permeable soils. Alternatively, suitable h_i can be achieved by placing the soil samples in equilibrium in an atmosphere with high relatively humidity. For instance, a pressure head of -6.0 10^5 cm can be obtained when a soil sample is stored at 20 ºC and 60% relative humidity (RILEM, 1980). Given that these atmospheric conditions are not difficult to accomplish, the initial tension considered from now on, both in the theoretical and experimental analysis, will be fixed to -6.0 10^5 cm.

Upward infiltration curves were longer in finer soils (Fig. 2). The α-n, K_s-n and K_s-α response surfaces calculated for the loamy sand, loam and clay soils showed, in all cases, an unique minimum (Fig. 2). These results indicate that K_s, α and n can be estimated from the inverse analysis of a single upward infiltration curve. However, the shapes of the error map varied depending on the soil type. For instance, the vertical and elongated α-n and K_s-n error maps observed in loamy sand makes that small changes in α or K_s promoted important variations of n. This can be related to the commonly abrupt $\theta(h)$ shapes observed in coarse soils, where small changes of the water retention slope make important variations in n. An opposite behavior was observed in clay, where the more horizontal α-n and K_s-n error maps made that minor changes in n promoted large variations of α and K. This dependence can be related to the flatter $\theta(h)$ shapes observed in fine soils, where large changes of α may induce small variations in the $\theta(h)$ slope. An intermediate behavior was observed in the loam soil (Fig. 2). These results, however, contrast with those obtained by Moret-Fernández et al. (2016a) and Peña-Sancho et al. (2017), where error maps calculated from the inverse analysis of an upward infiltration curve did not show an absolute minimum. These differences are explained because the soil initial condition used in those works was fixed in volumetric water content instead on pressure head. Under these circumstances, θ_i was set close to the measured θ_r, and h_i resulted free and dependent of α and n. These results indicate the initial soil tension is a key physical parameter in the capillarity processes. Moreover, the differences regarding to the above cited works could be also explained because of the steady-state phase at the end of the upward infiltration was not included in the inverse analysis. This assumption suggests that the measurement of the steady-state section is crucial to optimize the soil hydraulic properties.

Given the ill-conditioning of the error maps, the hydraulic parameters were estimated using an stochastic optimization method. The procedure was based on the ASSRS method, introducing preferential directions in the random search to increase convergence rate at the final stage of the optimization. The last ten successful points explored by the ASSRS method were linearized to approximate the direction that leads to the minimum. The satisfactory convergences of the optimization method in a loam soil, starting from four different initial values, indicate the proposed method allows accurate estimates of α, n and K_s, independently of the initial value (Fig. 3). A robust relationship (Fig. 4a) ($R^2 > 0.99$) was observed between the theoretical K_s, α and n and the corresponding optimized values for the eight synthetic soils of Table 1. In all cases, Φ (Eq. 6) was lower than $5.0\ 10^{-4}$ cm. The week dispersion found in K_s and α on clay can be related to the quasi-horizontal α-n and K_s-n error maps observed in this soil (Fig. 2), where small variations in n can make large changes in α and K. An also robust relationship (R^2 > 0.99) was found between the theoretical hydraulic properties and the intermediate values for a 0.02 mm error (Fig.4b), which corresponds with the experimental threshold error defined in Section 2.3. These results indicate that the proposed optimization can be satisfactorily applied to any kind of soil. The optimization, however, could be accelerated if initial hydraulic parameters (K_s', α' and n') close to the actual values were selected. For instance, these initial values could be obtained from the $K_s(S)$, $\alpha(S)$ and $n(S)$ regressions (Fig. 5), where S is integrated between θ_s and θ_i (Eq. 4). This relationship will be subsequently used to estimate K_s', α' and n' (Table 1) from S^* (Eq. 5).

3.2. Experimental validation

The S^* values estimated from the experimental infiltration curves (Eq. 5), together with the corresponding K_s', α' and n' are summarized in Table 2. Overall, good fittings were observed between the measured upward infiltration curves and the optimized ones (Table 2). For instance, Figure 6 compares the experimental vs. the best optimized curve, as well as the iterations followed by the optimization method applied to the experimental clay soil. A robust and significant relationship, with slope close to one and an average dispersion of 0.4% (Fig. 7), was observed between n measured with PC and the corresponding values estimated from the inverse analysis of the experimental infiltration curves (Fig. 7). This strong relationship could be associated to the fact that n is more related to the soil textural characteristics (Jirku et al., 2013), and hence, less affected by the influence of the wetting-drainage process on the soil structure (Moret-Fernández et al., 2016a). Similar results were obtained by Moret-Fernádnez et al. (2016b) and Moret-Fernández and Latorre (2017) with comparable upward infiltration methods. An also significant relationship, with slope close to one, was observed between the optimized K_s and the corresponding value obtained by Darcy. In this case, log(K_s) measured by Darcy was 2.5% higher than that estimated by the inverse analysis. A no-statistically significant relationship, with a slope away from the 1:1 line, was observed between α estimated with PC and that obtained with the infiltration method. Similar results were obtained by Moret-Fernández and Latorre (2017) with a comparable upward infiltration method. This behavior could be explained by the different wetting processes used in both methods (Moret-Fernández and Latorre, 2017), which may modify the contact angle of water with the soil particles, the amount of air entrapped in the pores, or the interconnection in the pore network (Bachmann and van der Ploeg, 2002; Maqsoud et al., 2004). Other explanation could be found in the empirical Gebrenegus and Ghezzehei (2011) hysteresis model, that could give an inaccurate description of α for a wetting process. An indirect confirmation for this hypothesis is given by the good correlation found in K_s and n, which are less affected by the hysteresis. A robust and significant relationship with slope close to one (Fig. 8) was observed between S calculated by applying the optimized α, n and K_s values to Eq.(4) and the corresponding S^* (Eq. 5) estimated from the upward infiltration curve. This satisfactory relationship corroborates the robustness of the inverse analysis.

CONCLUSIONS

This work demonstrates that K_s, α and n can be estimated from the inverse analysis of a single upward infiltration curve measured on a 5-cm high cylinder, when the initial soil tension is fixed to -6.0 10^5 cm. A robust and efficient optimization method was proposed and satisfactorily validated on synthetic and experimental sieved soils contained in 5-cm high cylinders covering in both cases a wide range of textures. Unlike previous methods, this new technique is simple, inexpensive, fast to implement, allows simultaneous estimates of all hydraulic parameters, can be applied to any kind of sieved soils and on the 5-cm high cores commonly employed for soil bulk density determination. However, new efforts should be done to test the method on heterogeneous and undisturbed soil samples, and to study the influence of the core length on the hydraulic properties estimation.

Acknowledgments

The authors are grateful to the Área de Informática Científica de la SGAI (CSIC) for their technical support in the numerical analysis and to Dra. M.V. López, R. Gracia and M.J. Salvador for they help in some laboratory tasks. The authors are also grateful to Dr. K. Seki and Dr. R. Angulo-Jaramillo for their advices in some theoretical aspects of the paper.

References

Avriel, M. Nonlinear Programming: Analysis and Methods. Englewood Cliffs (N.J.). Prentice-Hall, 2003.

Bachmann, J., van der Ploeg, R.R., 2002. A review on recent developments in soil water retention theory: interfacial tension and temperature effects. Journal of Plant Nutrition and Soil Science 165, 468–478.

Brooks, S.H., 1958. A Discussion of Random Methods for Seeking Maxima. Operations Research 6, 244-251.

Caldwell, T.G., Wohling, T., Young, M.H., Boyle, D.P., McDonald, E.V. 2013. Characterizing disturbed desert soils usingmultiobjective parameter optimization. Vadose Zone Journal 12 (1).

Carsel, R.F., Parrish, R.S., 1988. Developing joint probability distributions of soil water retention characteristics. Water Resources Research. 24, 755–769.

Dane J.H., Hopmans J.W. 2002. Water retention and storage. In Methods of Soil Analysis. Part. 4, Dane JH and Topp GC (editors). SSSA Book Series No. 5. Soil Science Society of America, Madison, WI.

Gebrenegus, T., Ghezzehei, T.A., 2011. An index for degree of hysteresis in water retention. Soil Science Society of America Journal 75, 2122–2127

Haverkamp, R., Ross, P.J., Smettem, K.R.J., Parlange, J.Y. 1994. Three dimensional analysis of infiltration from the disc infiltrometer. Part 2. Physically based infiltration equation. Water Resources Research 30, 2931-2935.

Haiping, Z., Yamada K. 1996. Estimation for urban runoff quality modeling. Water Science and Technology. 34, 49-54.

Horst, R., Romeijn, H.E. (Eds.), 2002. Handbook of Global Optimization, vol. 2. Springer Science & Business Media.

Hudson, D.B., Wierenga, P.J., Hills, R.G., 1996. Unsaturated hydraulic properties from upward flow into soil cores. Soil Science Society of America Journal 60, 388–396.

Jirku, V., Kodesová, R., Nikodem, A., Mühlhanselová, M., Zigová, A., 2013. Temporal variability of structure and hydraulic properties of topsoil of three soil types. Geoderma 204, 43–58.

Jones, S.B., Mace, R.W., Or, D., 2005. A time domain reflectometry coaxial cell for manipulation and monitoring of water content and electrical conductivity in variable saturated porous media. Vadose Zone Journal 4, 977–982.

Klute, A. 1986. Water retention curve: laboratory methods. In: Klute, A. (Ed.), Methods of Soil Analysis. Part 1. SSSA Book Series No. 9. Soil Science Society of America, Madison WI.

Klute, A. and Dirksen, C. 1986. Hydraulic conductivity and diffusivity: Laboratory methods. In: Klute, A. Ed., Methods of Soil Analysis - Part 1 - Physical and Mineralogical Methods, American Society of Agronomy, Madison, 687-734.

Lassabatere, L., Angulo-Jaramillo, R., Soria-Ugalde, J.M., Simunek, J., Haverkamp, R., 2009. Numerical evaluation of a set of analytical infiltration equations. Water Resources Research 45. http://dx.doi.org/10.1029/2009WR007941.

Latorre, B., Peña, C., Lassabatere L., Angulo-Jaramillo R., Moret-Fernández, D. 2015. Estimate of soil hydraulic properties from disc infiltrometer three-dimensional infiltration curve. Numerical analysis and field application. Journal of Hydrology 57, 1-12.

Maqsoud, A., Bussiere, B., Mbonimpa, M., Aubertin, M., 2004. Hysteresis effects on the water retention curve: a comparison between laboratory results and predictive models. In: Proc. 57th Can. Geotech. Conf. and the 5th joint CGS-IAH Conf., Quebec City. 24–27 October. The Canadian Geotechnical Soc., Richmond, BC, pp. 8–15.

Masaoka, N., Kosugi, K. 2018. Improved evaporation method for the measurement of the hydraulic conductivity of unsaturated soil in the wet range. Journal of Hydrology 563, 242–250.

Minasny, B., McBratney, A.B. 2000. Estimation of sorptivity from disc-permeameter measurements. Geoderma 95, 305-324.

Moret-Fernández, D., Latorre, B. 2017. Estimate of the soil water retention curve from the sorptivity and β parameter calculated from an upward infiltration experiment. Journal of Hydrology 544, 352–362.

Moret-Fernández, D., Peña-Sancho, C., López, M.V. 2016a. Influence of the wetting process on estimation of the water retention curve of tilled soils. Soil Research doi.org/10.1071/SR15274.

Moret-Fernández, D., Latorre, B., Angulo-Martínez, M. 2017a. Comparison of different methods to estimate the soil sorptivity from an upward infiltration curve. Catena 155, 86–92.

Moret-Fernández, D., Latorre, B., Peña-Sancho, C., Ghezzehei, T.A., 2016b. A modified multiple tension upward infiltration method to estimate the soil hydraulic properties. Hydrological Processes. http://dx.doi.org/10.1002/hyp.10827.

Moret-Fernández, D., Peña-Sancho, C., Latorre, B., Pueyo, Y., López, M.V. 2017b. Estimating the van Genuchten retention curve parameters of undisturbed soil from a single upward infiltration measurement. Soil Research doi.org/10.1071/SR16333

Moret-Fernández, D., Vicente, J., Latorre, B., Herrero, J., Castañeda, C., López, M.V., 2012. TDR pressure cell for monitoring water content retention curves on undisturbed soil samples. Hydrological Processes 26, 246–254.

Peña-Sancho, C., Ghezzehei, T.A., Latorrea, B., Moret-Fernández, D. 2017.Water absorption-evaporation method to estimate the soil hydraulic properties. Hydrological Science Journal 62, 1683-1693.

Philip J.R. 1957. The theory of infiltration: 4. Sorptivity and algebraic infiltration equations. Soil Sci. 84, 257-264.

Shao, M., Hudson, R. 1998. Integral method for estimating soil hydraulic properties. Soil Science Society of America Journal 62, 585-592.

Ramos, T., Gonçalves, M., Martins, J., van Genuchten,M.T., Pires, F., 2006. Estimation of soil hydraulic properties from numerical inversion of tension disk infiltrometer data. Vadose Zone Journal 5, 684–696.

Rashid, N., Askari, M., Tanaka, T., Simunek, J., van Genuchten, M., Th. 2015. Inverse estimation of soil hydraulic properties under oil palm trees. Geoderma 241–242, 306-312

RILEM (1980). Essais recommandés pour mesurer l'altération des pierres et évaluer l'efficacité des méthodes de traitement. Matériaux et Constructions, Bull. RILEM 13 (75), 175-253.

Schumer, M.A., Steiglitz, K. 1968. Adaptive step size random search. IEEE Transactions on Automatic Control. 13, 270-276.

Schindler, U. 1980. Ein Schnellverfahren zur Messung der Wasserleitfähigkeit im teilgesättigten Boden an Stechzylinderproben. Arch. Acker- Pflanzen- bau Bodenkd. 24, 1–7.

Schindler, U., Müller, L., 2006. Simplifying the evaporation method for quantifying soil hydraulic properties. Journal of Plant Nutrition and Soil Science 169, 623–629.

Schindler, U., Durner, W., von Unold, G., Müller, L., 2010. Evaporation method for measuring unsaturated hydraulic properties of soils: extending the measurement range. Soil Science Society of America Journal 74, 1071–1083.

Simunek, J., van Genuchten, M.T., 1997. Estimating unsaturated soil hydraulic properties from multiple tension disc infiltrometer data. Soil Science 162, 383–398.

Simunek, J., van Genuchten, M.T., 1996. Estimating unsaturated soil hydraulic properties from tension disc infiltrometer data by numerical inversion. Water Resources Research. 32, 2683–2696.

Simunek, J., Wendroth, O., van Genuchten, M.T., 1998. Parameter estimation analysis of the evaporation method for determining soil hydraulic properties. Soil Science Society of America Journal 62, 894–895.

Solone, R., Bittelli, M., Tomei, F., Morari, F., 2012. Errors in water retention curves determined with pressure plates: effects on the soil water balance. Journal of Hydrology 470, 65–75.

van Genuchten, M.T., 1980. A closed form equation for predicting the hydraulic conductivity of unsaturated soils. Soil Science Society of America Journal 44, 892–898.

Young, M.H., Karagunduz, A., Siumunek, J., Pennell, K.D., 2002. A modified upward infiltration method for characterizing soil hydraulic properties. Soil Science Society of America Journal 66, 57–64.

Wind, G.P., 1968. Capillary conductivity data estimated by a simple method. In: Rijtema, P.E., Wassink, H. (Eds.), Water in the unsaturated zone. Vol. 1. Proc. Wageningen Symp. June 1966. Int. Assoc. Scientific Hydrol. Gentbrugge, Belgium, pp. 181–191.

Figures captions

Figure 1. Water retention curve and response surfaces for the *α*-*n*, K_s-*n* and K_s-*α* planes calculated on a theoretical loam soil for two different initial soil tensions (h_i) (Table 1). Contour lines indicate errors of 0.05, 0.1, 0.2, 0.5, 1, 2 and 5 mm, respectively, red line is the contour line for an error of 0.02 mm and blue circle denotes the theoretical value.

Figure 2. Simulated cumulative infiltration curves and response surfaces for the *α*-*n*, K_s-*n* and K_s-*α* planes calculated for theoretical loamy sand, loam and clay soils (Table 1). Contour lines indicate errors of 0.05, 0.1, 0.2, 0.5, 1, 2 and 5 mm, respectively, red line is the contour line for an error of 0.02 mm and blue circle denotes the theoretical value.

Figure 3. Convergence of the optimization to the K_s, *α* and *n* values of a theoretical loam soil from four different initial values.

Figure 4. Relationship between the theoretical K_s, *α* and *n* of Table 1 and the corresponding values obtained with the optimization for (a) the best result and (b) the intermediate iteration reaching 0.02 mm error.

Figure 5. Experimental relationship between *S* (Eq. 4) and K_s, *α* and *n* of the theoretical soils of Table 1.

Figure 6. (a) Experimental (circles) and optimized (red line) upward infiltration curve and (b) convergence of K_s, *α* and *n* during the optimization of the experimental sieved clay soil.

Figure 7. Relationship between K_s, α and n estimated on the experimental soils with the Darcy's and PC methods and the corresponding hydraulic values estimated from the inverse analysis (opt) of the upward infiltration curves.

Figure 8. Relationship between the sorptivity (S) of the experimental soils estimated from Eq.(4) and the optimized α, n and K_s values and the corresponding sorptivity estimated with Eq.(5) (S^*).

Table 1. Theoretical values of initial (θ_i), saturated (θ_s) and residual (θ_r) water content, α and n parameters of the van Genuchten (1980) water retention curve, saturated hydraulic conductivity (K_s), sorptivity calculated with Eq. (4) (S) and estimated from Eq. (5) (S^*), and K_s, α and n parameters (K_s', α' and n') estimated from $K_s(S)$, $\alpha(S)$ and $n(S)$ relationships (Fig. 3).

	θ_i	θ_r	θ_s	α	n	K_s	S	S^*	α'	n'	K_s'
	cm^3 cm^{-3}			cm^{-1}		cm s^{-1}	cm s$^{-0.5}$		cm^{-1}		cm s^{-1}
Loamy sand	0.057	0.057	0.41	0.124	2.28	4.05 10^{-3}	0.1025	0.1021	0.106	2.28	3.58 10^{-03}
Sandy loam	0.065	0.065	0.41	0.075	1.89	1.23 10^{-3}	0.0634	0.0635	0.076	1.87	1.42 10^{-03}
Loam	0.079	0.078	0.43	0.036	1.56	2.88 10^{-4}	0.0367	0.0366	0.047	1.55	8.05 10^{-05}
Silt	0.048	0.034	0.46	0.016	1.37	6.93 10^{-5}	0.0238	0.0235	0.031	1.38	1.67 10^{-04}
Sandy clay loam	0.102	0.100	0.39	0.059	1.48	3.64 10^{-4}	0.0309	0.0307	0.036	1.48	2.79 10^{-04}
Clay loam	0.112	0.095	0.41	0.019	1.31	7.22 10^{-5}	0.0174	0.0176	0.022	1.29	7.40 10^{-05}
Silty clay loam	0.135	0.089	0.43	0.010	1.23	1.99 10^{-5}	0.0104	0.0105	0.013	1.19	1.68 10^{-05}
Clay	0.213	0.068	0.38	0.008	1.09	5.55 10^{-5}	0.0076	0.0078	0.009	1.17	3.55 10^{-06}

Table 2. Soil particle size, gypsum and organic carbon content, OC, bulk density, ρ_b, residual, θ_r, and saturated, θ_s, volumetric water content, saturated hydraulic conductivity, K_s', α' and n' calculated form the estimated sorptivity (S^*), and error, Φ (Eq. 6), obtained by the inverse analysis of the experimental soils

Treatment *	*Sand*	*Silt*	*clay*	*Gypsum*	*OC*	ρ_b	θ_r	θ_s	S *	K_s'	α'	n'	Φ
	g kg^{-1}					g cm^{-3}	m^3 m^{-3}		cm s$^{-0.5}$	cm s^{-1}	cm^{-1}		mm
Sand	1000	-	-	-	-	1.64	0.02	0.35	0.210	1.65 10^{-2}	0.175	2.97	0.08
Loam	280	470	250	-	11.7	1.25	0.03	0.47	0.074	2.05 10^{-3}	0.086	1.99	0.11
Clay loam	205	497	298	-	19.9	1.33	0.03	0.44	0.065	1.58 10^{-3}	0.077	1.89	0.15
Silt-Gypseous	316	591	129	703	1.50	1.02	0.01	0.37	0.042	6.61 10^{-4}	0.052	1.62	0.08
Clay	151	344	465	-	12.4	1.30	0.03	0.40	0.041	6.29 10^{-4}	0.051	1.60	0.09

* S estimated from the inverse analysis of the upward infiltration curve using Eq. (5)

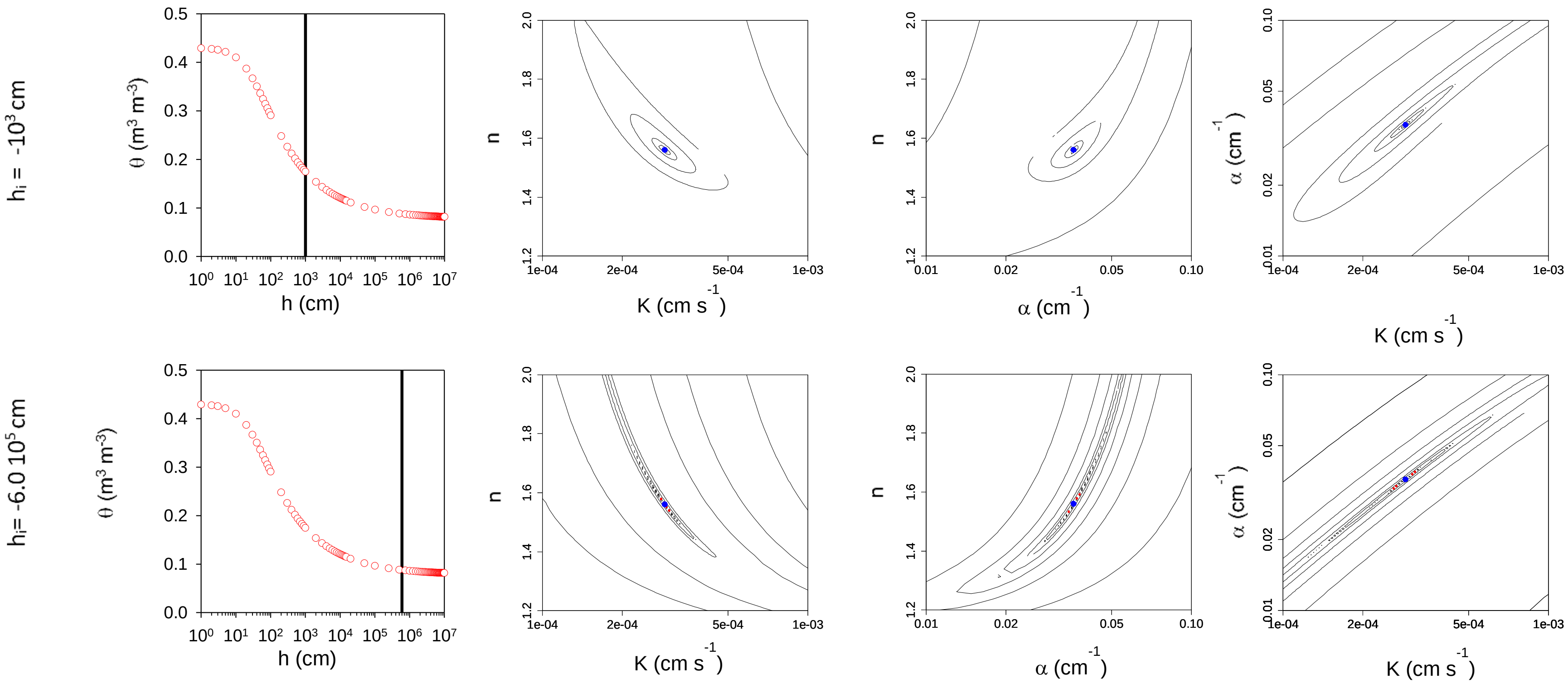

Figure 1.

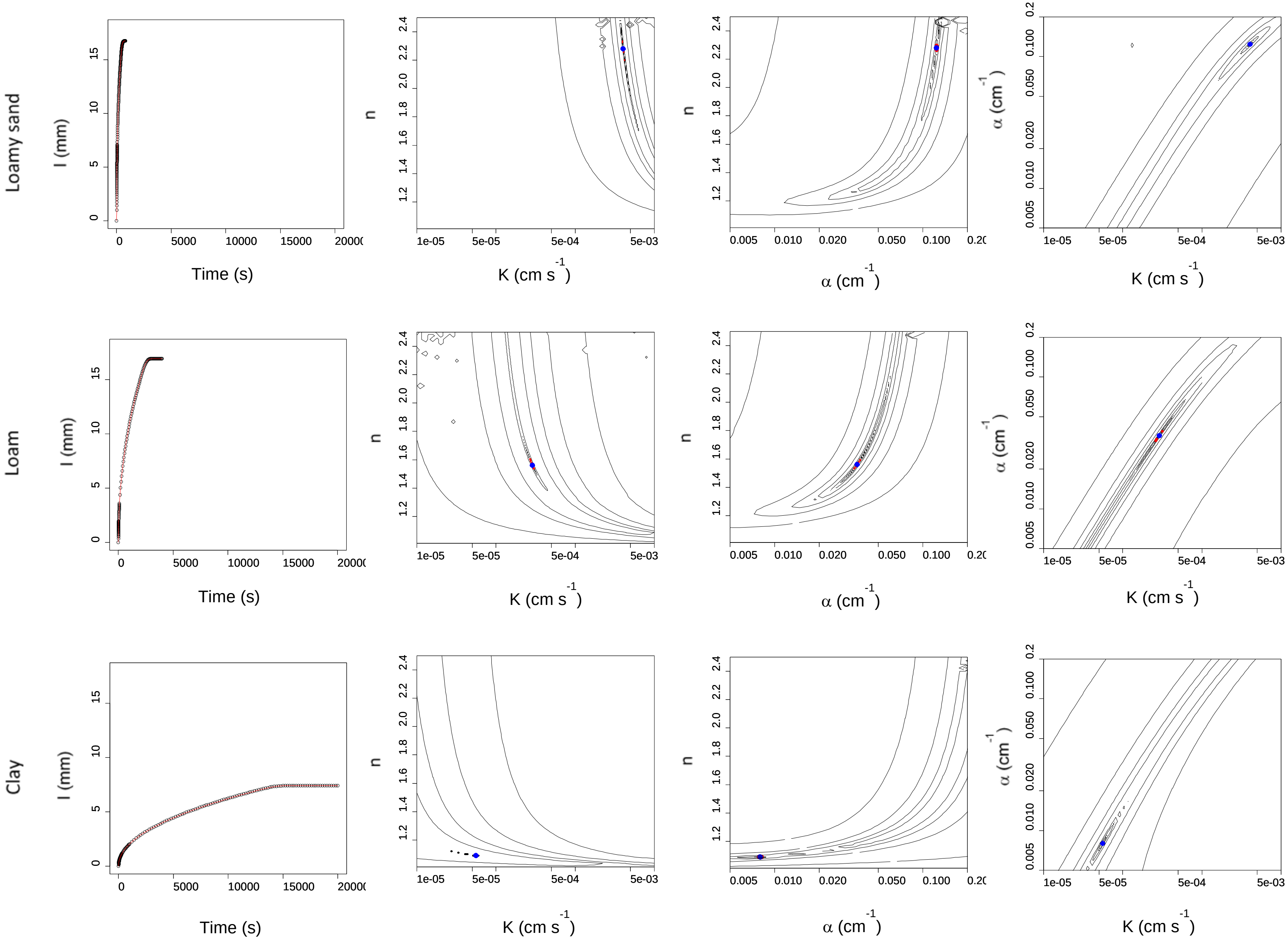

Figure 2.

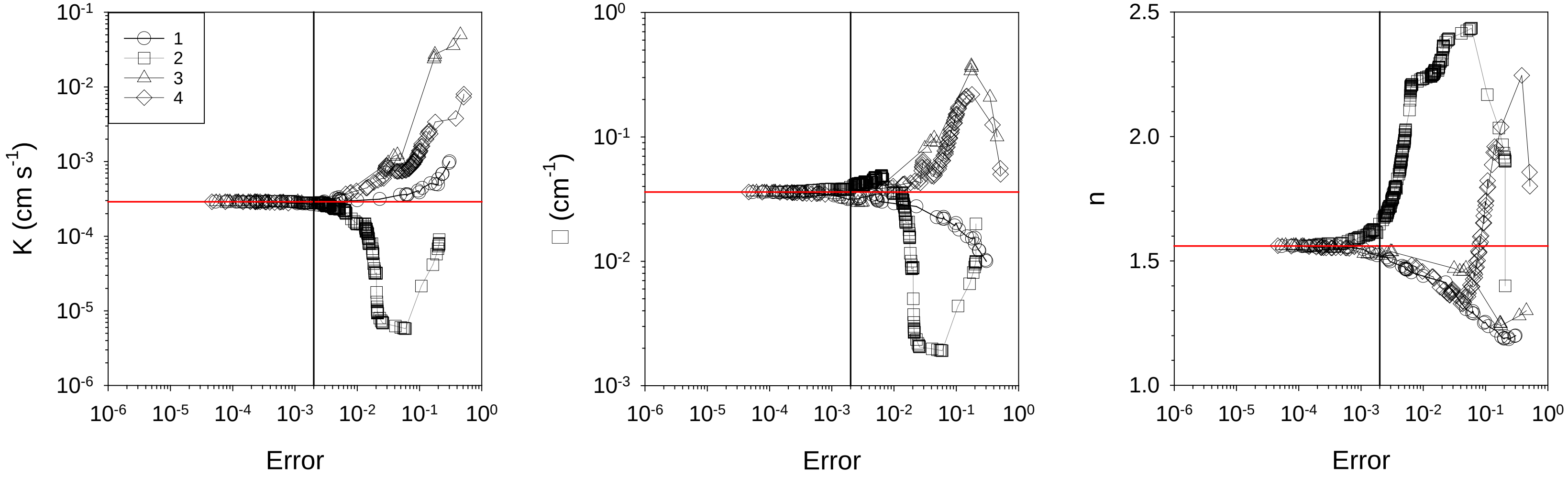

Figure 3.

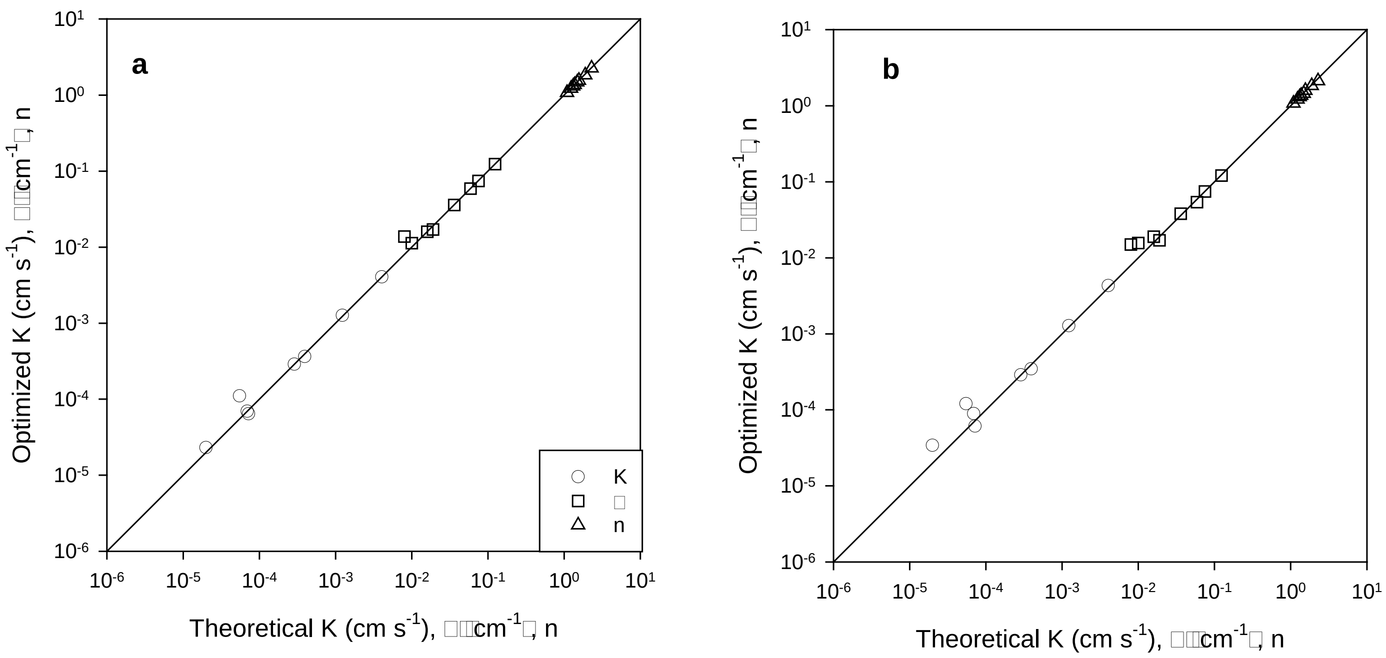
a
b
Optimized K (cm s-1), cm-1, n
Theoretical K (cm s-1), cm-1, n
K
n
10-6
10-5
10-4
10-3
10-2
10-1
100
101

Figure 4

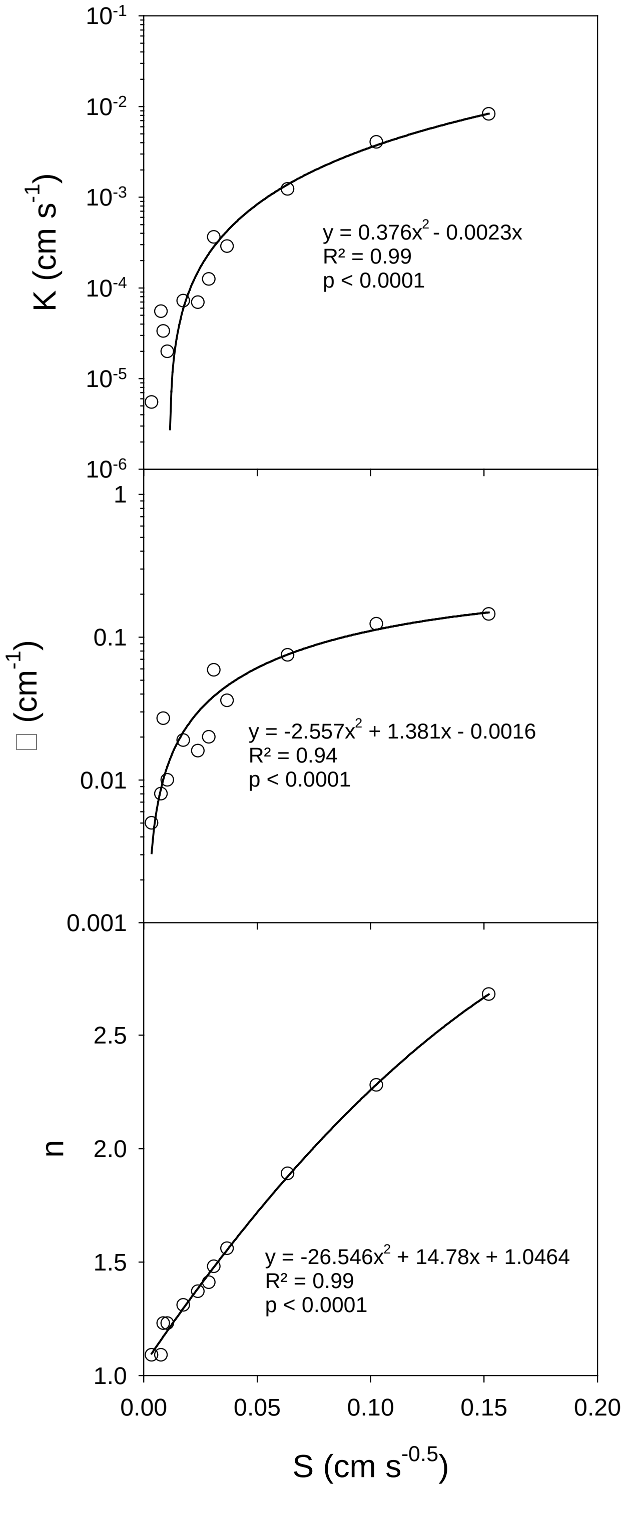
10-1
10-2
10-3
10-4
10-5
10-6
K (cm s-1)
y = 0.376x2 - 0.0023x
R² = 0.99
p < 0.0001
1
0.1
0.01
0.001
(cm-1)
y = -2.557x2 + 1.381x - 0.0016
R² = 0.94
p < 0.0001
2.5
2.0
1.5
1.0
n
y = -26.546x2 + 14.78x + 1.0464
R² = 0.99
p < 0.0001
0.00
0.05
0.10
0.15
0.20
S (cm s-0.5)

Figure. 5

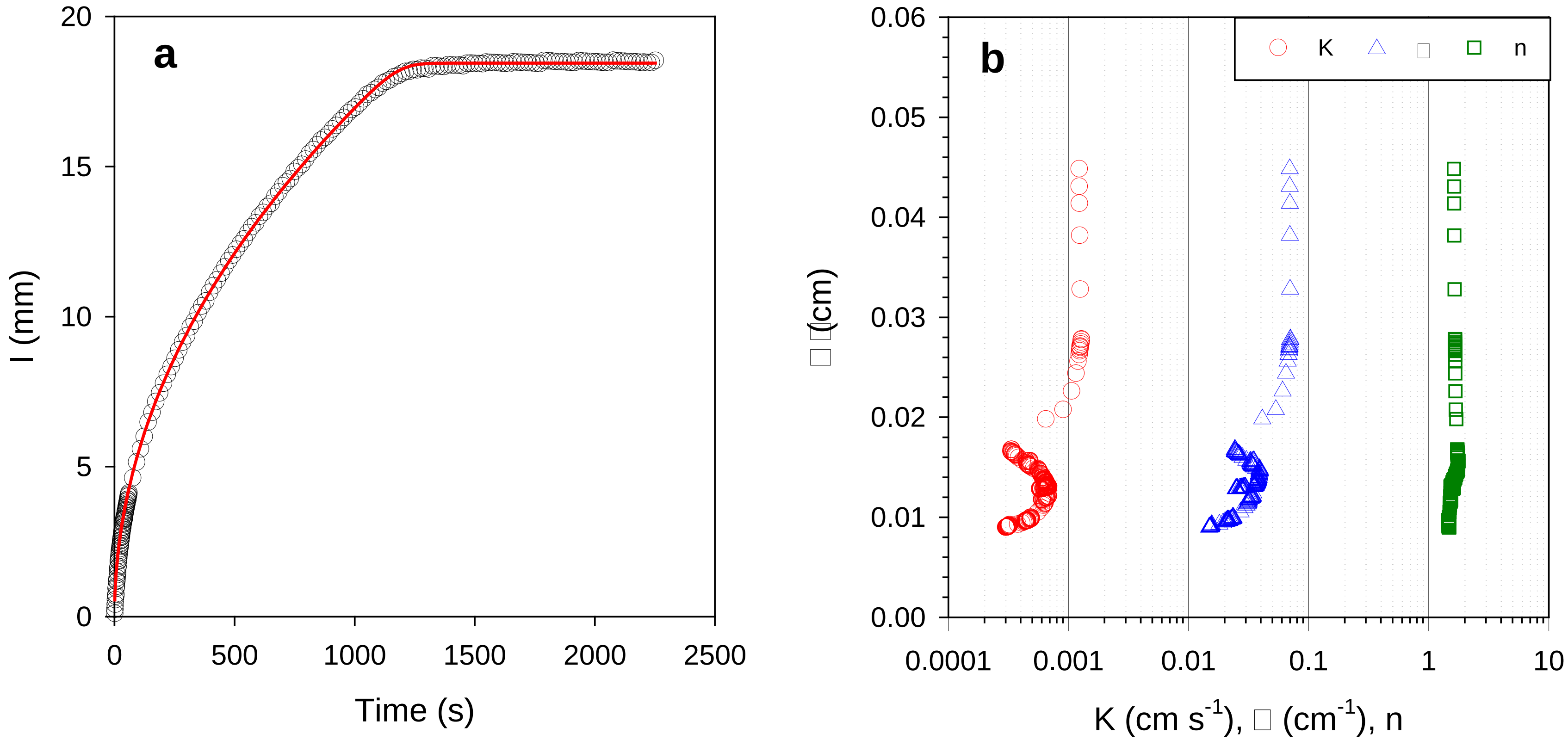
a
20
15
10
5
0
l (mm)
0
500
1000
1500
2000
2500
Time (s)
b
0.06
0.05
0.04
0.03
0.02
0.01
0.00
(cm)
K
n
0.0001
0.001
0.01
0.1
1
10
K (cm s-1), (cm-1), n

Figure 6.

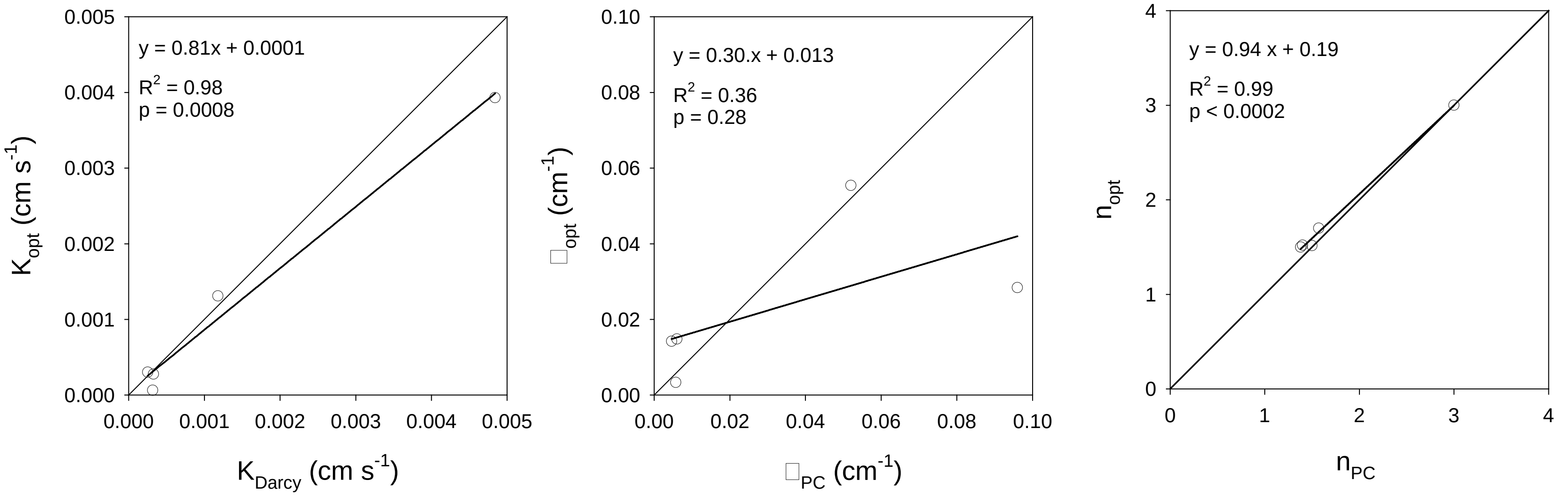

y = 0.81x + 0.0001
R2 = 0.98
p = 0.0008
Kopt (cm s-1)
KDarcy (cm s-1)
0.000
0.001
0.002
0.003
0.004
0.005
y = 0.30.x + 0.013
R2 = 0.36
p = 0.28
opt (cm-1)
PC (cm-1)
0.00
0.02
0.04
0.06
0.08
0.10
y = 0.94 x + 0.19
R2 = 0.99
p < 0.0002
nopt
nPC
0
1
2
3
4

Figure 7.

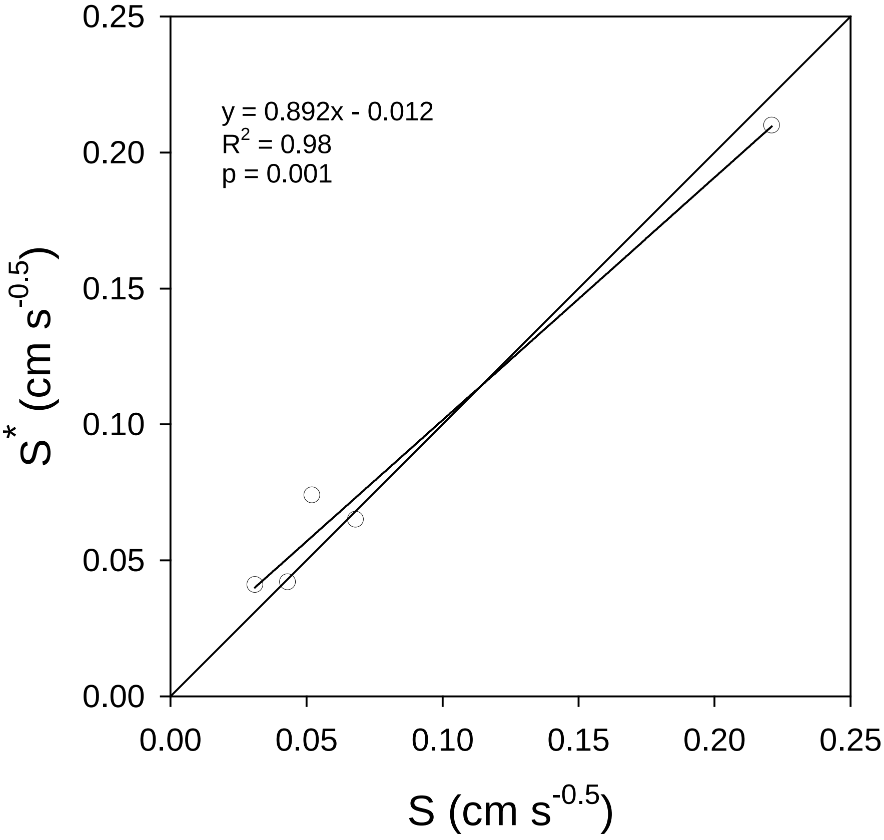
y = 0.892x - 0.012
R2 = 0.98
p = 0.001
S* (cm s-0.5)
S (cm s-0.5)
0.00
0.05
0.10
0.15
0.20
0.25

Figure 8.